

On Richtmyer-Meshkov unstable dynamics of three-dimensional interfacial coherent structures with time-dependent acceleration

D.L. Hill^{1, a)} and S.I. Abarzhi^{1, b)}

University of Western Australia, Perth, WA, 6009, Australia

(Dated: 2 December 2019)

Richtmyer-Meshkov instability (RMI) plays an important role in many areas of science and engineering, from supernovae and fusion to scramjets and nano-fabrication. Classical Richtmyer-Meshkov instability is induced by a steady shock and impulsive acceleration, whereas in realistic environments the acceleration is usually variable. We focus on RMI induced by acceleration with power-law time-dependence and apply group theory to solve the long-standing problem. For early-time dynamics, we find the dependence of the growth-rate on the initial conditions and show that it is independent of the acceleration parameters. For late-time dynamics, we find a continuous family of regular asymptotic solutions, including their curvature, velocity, Fourier amplitudes, and interfacial shear, and we study their stability. For each solution, the interface dynamics is directly linked to the interfacial shear, the non-equilibrium velocity field has intense fluid motion near the interface and effectively no motion in the bulk. The quasi-invariance of the fastest stable solution suggests that nonlinear coherent dynamics in RMI is characterized by two macroscopic length-scales - the wavelength and the amplitude, in agreement with observations. The properties of a number of special solutions are outlined, these being respectively, the Atwood, Taylor, convergence, minimum-shear, and critical bubbles, among others. We also elaborate new theory benchmarks for future experiments and simulations.

I. INTRODUCTION

Rayleigh-Taylor instability (RTI) develops at the fluid interface when fluids of different densities are accelerated against their density gradients; Richtmyer-Meshkov instability (RMI) develops when the acceleration is induced by a shock and is impulsive¹⁻⁴. Intense interfacial Rayleigh-Taylor (RT) / Richtmyer-Meshkov (RM) mixing of the fluids ensues with time^{5,6}. RTI/RMI and RT/RM mixing play an important role in a broad range of processes in nature and technology, including stellar evolution and plasma fusion, and in the fossil fuel industry⁷⁻¹³. In this work we study the long-standing problem of RMI with variable acceleration¹⁴. We employ group theory to solve the boundary value problem for the early-time and late-time RMI¹⁵, directly link RM dynamics to the interfacial shear, identify its invariance properties, and reveal the interfacial and multi-scale character of RM dynamics. Our theory finds similarities and differences between RM and RT dynamics with variable accelerations¹⁴, agrees with existing observations, and elaborates new diagnostic benchmarks for experiment and simulation.

RMI with variable acceleration commonly occur in fluids, plasmas, and materials⁷⁻¹⁴: RMI leads to the appearance of light-years-long structures in clouds of molecular hydrogen, influences the formation of hot spots in inertial confinement fusion, controls combustion processes in scramjets, and drives material transformation under impact in nano-fabrication. In these vastly different physical conditions, RM flows have similar qualitative features of their evolution. The post-shock RM dynamics is a superposition of two motions. These are the background motion of the fluid bulk and the growth of the interface perturbations^{1,2,6,16-19}. In the background motion,

both fluids and their interface move as a whole in the direction of the transmitted shock. This motion occurs even for an ideally planar interface and is supersonic for strong shocks. The growth of the interface perturbations is due to impulsive acceleration by the shock; it develops only when the flow fields are perturbed; its growth rate is subsonic and the associated motion is incompressible^{1,2,6,16-23}. The growth rate is constant initially and decays with time later. The RM unstable interface is transformed to a composition of small-scale shear-driven vortical structures and a large-scale coherent structure of bubbles and spikes, where a bubble (spike) is a portion of the light (heavy) fluid penetrating the heavy (light) fluid. Small-scale non-uniform structures appear also in the bulk, including hot and cold spots, high and low pressure regions, cumulative jets, checker-board velocity patterns^{5,6,16-20}. Over time, self-similar RM mixing develops, and energy supplied initially by the shock gradually dissipates^{5,6,14-23}.

RMI/RTI and RM/RT mixing are a challenge to study in theory, experiments and simulations¹⁴⁻³⁴. As regards the general theory, we have to develop new approaches for non-equilibrium multi-scale RM/RT dynamics, capture symmetries of these RM/RT dynamics and identify properties of their asymptotic solutions^{5,14,15,25-30}. Experimental work requires one to meet tight requirements on the flow implementation, diagnostics and control^{2,6,20-24}. Simulations must employ highly accurate numerical methods, requiring massive computations in order to capture shocks, track interfaces, and accurately model small-scale processes^{16-19,30-34}. In addition, a substantial span of temporal and spatial scales is required for bias-free interpretation of experimental and numerical data describing RM/RT evolution¹⁴⁻³⁴. Significant success has recently been achieved in our understanding of RMI and RTI, as well as RM and RT mixing^{5,14,15,25}. In particular, the group theory approach has uncovered the multi-scale character of nonlinear RMI and RTI, and found an order in RT mixing with constant acceleration, thus explaining observations^{5,14,15,25}.

In realistic environments, RT and RM flows are usually

^{a)}Electronic mail: des.hill@uwa.edu.au

^{b)}Electronic mail: snezhana.abarzhi@gmail.com

driven by variable acceleration^{8–14} and only limited information is currently available on RM and RT dynamics under these conditions¹⁴. An important special case is that of acceleration with power-law time-dependence, because power-law functions may lead to new scaling properties of the dynamics and can be used to adjust the acceleration's time-dependence in applications^{8–14,35,36}. For such accelerations, the early-time and late-time scale-dependent dynamics can be of RM or RT type, depending on the exponent in the acceleration power-law^{14,37}. Specifically, the interfacial dynamics is driven by the acceleration and is of RT-type for exponents larger than (-2) , and is driven by the initial growth-rate and is of RM-type otherwise^{14,37}. A self-similar mixing regime ensues over time^{5,6}.

In this work, we study the long-standing problem of RMI with variable acceleration for a three-dimensional spatially extended periodic flow. We apply group theory with the spatial symmetry group of the square to solve the boundary value problem involving boundary conditions at the interface and the outside boundaries, and the initial value problem^{5,14,15,25,37}. For early-time dynamics, we find the dependence of the RMI growth-rate on the initial conditions and show that it is independent of the acceleration parameters. For late-time dynamics, we directly link the interface dynamics to the interfacial shear, find a continuous family of regular asymptotic solutions, and study the stability of the solutions in this family. For each of the family of solutions, the perturbed velocity field has intense fluid motion near the interface and effectively no motion in the bulk. We identify parameters of a number of special solutions, these being the Atwood bubble, which is flat and is the fastest, and respectively, the Taylor, convergence, minimum-shear, and critical bubbles. In each case we give the curvature, velocity, Fourier amplitudes, and interfacial shear. The Atwood bubble has a quasi-invariance property suggesting that nonlinear coherent RM dynamics is set by the interplay of two macroscopic length-scales - the wavelength and the amplitude. Our theory agrees with existing observations, and elaborates new benchmarks for observations^{6,8–14,20–23}.

II. THE METHOD OF SOLUTION

A. The governing equations

The dynamics of ideal fluids is governed by conservation of mass, momentum and energy:

$$\begin{aligned} \frac{\partial \rho}{\partial t} + \frac{\partial}{\partial x_i}(\rho v_i) &= 0, \\ \frac{\partial}{\partial t}(\rho v_j) + \frac{\partial}{\partial x_i}(\rho v_i v_j) + \frac{\partial P}{\partial x_j} &= 0, \\ \frac{\partial E}{\partial t} + \frac{\partial}{\partial x_i}((E+P)v_i) &= 0, \end{aligned} \quad (1)$$

where $j = 1, 2, 3$, $(x_1, x_2, x_3) = (x, y, z)$ are the spatial coordinates, t is time, (ρ, \mathbf{v}, P, E) are the fields of density ρ , velocity \mathbf{v} , pressure P and energy $E = \rho(e + \mathbf{v}^2/2)$, where e is the specific internal energy²⁷. The flow fields are understood as post-shock in the inertial frame of reference moving with the velocity of the background motion, in the direction of the transmitted shock.

We consider immiscible, inviscid fluids of differing densities, separated by a sharp interface. It is required that momentum must be conserved at the interface and that there can be no mass flow across it. Hence the boundary conditions at the interface are

$$[\mathbf{v} \cdot \mathbf{n}] = 0, \quad [P] = 0, \quad [\mathbf{v} \cdot \boldsymbol{\tau}] = \text{arbitrary}, \quad [W] = \text{arbitrary}, \quad (2)$$

where $[\dots]$ denotes the jump of functions across the interface; \mathbf{n} and $\boldsymbol{\tau}$ are the normal and tangential unit vectors of the interface with $\mathbf{n} = \nabla \theta / |\nabla \theta|$ and $\mathbf{n} \cdot \boldsymbol{\tau} = 0$; $W = e + P/\rho$ is the specific enthalpy; $\theta = \theta(x, y, z, t)$ is a local scalar function, with $\theta = 0$ at the interface and $\theta > 0$ ($\theta < 0$) in the bulk of the heavy (light) fluid, indicated hereafter by subscript $h(l)$.

The heavier fluid sits above the lighter fluid and the entire system is subject to a time-dependent acceleration field, directed from the heavy to the light fluid (and transmitted in the direction of the shock). The acceleration is the power-law function of time, $\mathbf{g} = (0, 0, -g)$ where $g = Gt^a$. Here a is the acceleration exponent, and $G > 0$ is the acceleration pre-factor^{28,38,39}. Their dimensions are $[G] = ms^{-(a+2)}$ and $[a] = 1$. This modifies the pressure field.

We assume that the outside boundaries do not influence the dynamics and there are no mass sources. Hence at the outside boundaries of the domain, the boundary conditions are

$$\lim_{z \rightarrow \infty} \mathbf{v}_h = \mathbf{0}, \quad \lim_{z \rightarrow -\infty} \mathbf{v}_l = \mathbf{0}. \quad (3)$$

B. Large-scale coherent structures

RM large-scale coherent structures are the arrays of bubbles and spikes periodic in the plane normal to the acceleration direction. At large scales the flow can be assumed to be irrotational in the bulk. We also assume that the fluids are incompressible and hence that the velocities are expressible in terms of scalar potentials $\Phi_h(x, y, z, t)$ and $\Phi_l(x, y, z, t)$. Because the fluids are ideal these are harmonic, with $\nabla^2 \Phi_h = 0$ in $\theta > 0$ and $\nabla^2 \Phi_l = 0$ in $\theta < 0$.

For convenience we perform the calculations in the non-inertial frame of reference moving with velocity $v(t)$ in the z -direction, where $v(t) = \partial z_0 / \partial t$ and z_0 are the velocity and position (amplitude) in the inertial reference frame at a regular point of the interface, such as the tip of a bubble or a spike. Then the interface function is $\theta(x, y, z, t) = z - z^*(x, y, t) = 0$, and the interface conditions are

$$\begin{aligned} \rho_h \left(\nabla \Phi_h \cdot \mathbf{n} + \frac{\dot{\theta}}{|\nabla \theta|} \right) &= 0 = \rho_l \left(\nabla \Phi_l \cdot \mathbf{n} + \frac{\dot{\theta}}{|\nabla \theta|} \right), \\ \rho_h \left(\frac{\partial \Phi_h}{\partial t} + \frac{|\nabla \Phi_h|^2}{2} + \left(g(t) + \frac{dv}{dt} \right) z \right) & \end{aligned}$$

$$= \rho_l \left(\frac{\partial \Phi_l}{\partial t} + \frac{|\nabla \Phi_l|^2}{2} + \left(g(t) + \frac{dv}{dt} \right) z \right),$$

$$\nabla \Phi_h \cdot \boldsymbol{\tau} - \nabla \Phi_l \cdot \boldsymbol{\tau} = \text{arbitrary} \quad (4)$$

In the non-inertial reference frame, the outside boundary condition (3) takes the form

$$\nabla \Phi_h \Big|_{z \rightarrow \infty} = (0, 0, -v(t)), \quad \nabla \Phi_l \Big|_{z \rightarrow \infty} = (0, 0, -v(t)). \quad (5)$$

C. The dynamical system

The length scale is $1/k$, where k is a wavenumber, with $k = 2\pi/\lambda$ and λ being the wavelength. There are two natural time scales in the problem³⁷. These are $\tau_g = (kG)^{-1/(a+2)}$ and $\tau_0 = 1/kv_0$, where v_0 is some initial growth rate. For $a < -2$, $\tau_0 \ll \tau_g$ and the fastest process is set by the initial growth-rate; this is the initial growth-rate driven Richtmyer-Meshkov type dynamics³⁷. Hence, we set the time scale to be $\tau = \tau_0$ and we will consider the flow for $t \gg t_0$ with $t_0 \gg \tau$, that is, sufficiently later than the initial shock. The Atwood number $A = (\rho_h - \rho_l)/(\rho_h + \rho_l)$ parametrises the ratio of densities of the fluids, and $0 < A < 1$.

The periodic nature of the large-scale coherent structure can be accommodated by appealing to the theory of space groups^{5,14,15,25}. As a specific example, we focus on three-dimensional flow with square symmetry. The details of the procedure are given elsewhere^{5,14,15,19,25,27,37,40,41}. The symmetry group dictates a specific Fourier series (an irreducible representation of the group) which can be used to solve the nonlinear boundary value problem Eq. (4), Eq. (5). We then make spatial expansions in the vicinity of the tip of a regular point on the interface. This approach reduces the governing equations to a dynamical system of ordinary differential equations in terms of interface variables and Fourier moments^{5,14,15,25,27,39}.

The corresponding potentials are

$$\Phi_h(x, y, z, t) = \sum_{m,n=0}^{\infty} \Phi_{mn}(t) \left(\frac{\cos(mkx) \cos(nky) e^{-\alpha_{mn}kz}}{\alpha_{mn}k} + z \right)$$

$$+ f_h(t),$$

$$\Phi_l(x, y, z, t) = \sum_{m,n=0}^{\infty} \tilde{\Phi}_{mn}(t) \left(\frac{\cos(mkx) \cos(nky) e^{\alpha_{mn}kz}}{\alpha_{mn}k} - z \right)$$

$$+ f_l(t), \quad (6)$$

where $\alpha_{mn} = \sqrt{m^2 + n^2}$, m and n are integers, $k = \frac{2\pi}{\lambda}$ is the wavenumber, Φ_{mn} and $\tilde{\Phi}_{mn}$ are the Fourier amplitudes for the heavy and light fluids respectively, with $\Phi_{00} = \tilde{\Phi}_{00} = 0$, and $f_h(t)$ and $f_l(t)$ are time-dependent functions. Symmetry requires that $\Phi_{mn} = \Phi_{nm}$ and $\tilde{\Phi}_{mn} = \tilde{\Phi}_{nm}$. The sign of the z term is determined by the boundary condition Eq. (5).

For application of symmetry groups in Rayleigh-Taylor and Richtmyer-Meshkov instability, the reader is referred to other works^{5,14,15,19,25,27,37,40,41}.

In order to examine the local behavior of the interfacial dynamics in the vicinity of the bubble tip, we expand the interface function in a power series in the vicinity of a regular point of the interface (e.g. the tip of the bubble or spike). In the moving frame of reference, this is

$$z^*(x, y, t) = \sum_{N=1}^{\infty} \sum_{i+j=N} \zeta_{ij}(t) x^{2i} y^{2j}, \quad (7)$$

where $\zeta_{ij}(t) = \zeta_{ji}(t)$ due to symmetry, $\zeta_1(t) = \zeta_{10}(t)$ is the principal curvature at the regular point, and $N = i + j$ is the order of the approximation. To lowest order (that is, $N = 1$), the interface is $z^*(x, y, t) = \zeta_1(t)(x^2 + y^2)$.

The Fourier series and interface function are substituted into the governing equations and the resulting expressions expanded as Taylor series. This yields a system of ordinary differential equations for $\Phi_m(t)$, $\tilde{\Phi}_m(t)$ and $\zeta_{ij}(t)$. We may express the potentials in terms of moments

$$M_{a,b,c}(t) = \sum_{mn} \Phi_{mn}(t) (mk)^a (nk)^b (\alpha_{mn}k)^c$$

and

$$\tilde{M}_{a,b,c}(t) = \sum_{mn} \tilde{\Phi}_{mn}(t) (mk)^a (nk)^b (\alpha_{mn}k)^c$$

We note that by symmetry, $M_{a,b,c} = M_{b,a,c}$ and $M_{a+2,b,c} + M_{a,b+2,c} = M_{a,b,c+2}$ and similarly for \tilde{M} . At $N = 1$, we abbreviate the series to second order in x and y , and first order in z since $z^*(x, y, t)$ is quadratic in x and y .

The boundary conditions at the interface and at the outside boundaries of the domain become

$$\dot{\zeta}_1 = 4M_1 \zeta_1 + \frac{M_2}{2}, \quad \dot{\zeta}_1 = 4\tilde{M}_1 \zeta_1 - \frac{\tilde{M}_2}{2}, \quad (8)$$

$$(1+A) \left(\frac{\dot{M}_1}{2} + \zeta_1 \dot{M}_0 - \frac{M_1^2}{2} \right) = (1-A) \left(\frac{\dot{\tilde{M}}_1}{2} - \zeta_1 \dot{\tilde{M}}_0 - \frac{\tilde{M}_1^2}{2} \right), \quad (9)$$

$$M_1 - \tilde{M}_1 = \text{arbitrary} \quad (10)$$

$$M_0 = -\tilde{M}_0 = -v(t) \quad (11)$$

where $M_0 = M_{0,0,0}$, $M_1 = M_{2,0,-1}$ and $M_2 = M_{2,0,0}$. This representation in terms of moments M and \tilde{M} , and the interface variable ζ_1 , accommodates the nonlocal nature of the nonlinear dynamics and enables us to investigate the interplay of harmonics and derive regular asymptotic solutions.

Our expressions can account for any number of harmonics in any order. Previous work with either $a = 0$ or $G = 0$ has demonstrated that the $N = 1$ solutions properly capture the physical behaviour^{5,14,15,25,27,38-40}. Hence we consider only the case when $N = 1$.

III. RESULTS

As previously mentioned, we are considering arrays of bubbles and spikes periodic in the plane normal to the acceleration direction. Bubbles are intrusions of the lighter fluid into the heavier fluid and as such move upwards and are concave down. Spikes are intrusions of the heavier fluid into the lighter fluid and as such move downwards and are concave up. We note that the dynamics of bubbles is regular, whereas that of spikes is singular. Our early-time analysis applies in both cases. Here, we focus our attention on the later-time dynamics of bubbles. That of spikes will be discussed elsewhere.

A. The early-time regime, $t - t_0 \ll \tau$

In the early-time regime, the system can be linearised and only first-order harmonics are needed, that is, the moments retain only one Fourier amplitude. The initial conditions at time t_0 are the initial curvature $\zeta_1(t_0)$ and velocity $v(t_0)$, and $|v_0(t)| = v_0$.

For a broad class of initial conditions, integration of the governing equations is a challenge. The solution can be found^{4,14,35,37} when the amplitude of the initial perturbation is small $\tau k |v_0| \ll 1$, and the interface is nearly flat $|\zeta_1/k| \ll 1$. The system reduces to

$$\dot{\zeta}_1 = \left(\frac{k^2}{4}\right) M_0, \quad \dot{M}_0 = \frac{Ak}{2} M_0^2. \quad (12)$$

When $t - t_0 \ll \tau = 1/kv_0$, only first order harmonics are retained in moments, that is, $M_0 = 2\Phi_{10}$, $\tilde{M}_0 = 2\tilde{\Phi}_{10}$; $M_n = k^n \Phi_{10}$, $\tilde{M}_n = k^n \tilde{\Phi}_{10}$, $n = 1, 2$. For an almost flat interface the solution is

$$-\frac{\zeta}{k} = \frac{1}{2A} \ln \left(C_2 \frac{t}{\tau} + C_1 \right), \quad v = \frac{4}{k} \frac{d}{dt} \left(-\frac{\zeta}{k} \right), \quad (13)$$

where C_1 and C_2 are integration constants defined by the initial conditions $\zeta_0 = \zeta(t_0)$ and $v_0 = v(t_0)$ with $\zeta_0/k \ll 1$ and $\tau k |v_0| \ll 1$ ^{4,14,35}. First-order analysis of the very-early-time ($t \sim t_0$) dynamics yields

$$\zeta - \zeta_0 \sim -\frac{k^2 v_0}{4} (t - t_0), \quad v - v_0 \sim -\frac{Akv_0^2}{2} (t - t_0) \quad (14)$$

which suggests that the positions of bubbles ($\zeta \leq 0, v \geq 0$) and spikes ($\zeta \geq 0, v \leq 0$) are defined by the initial velocity field, with bubbles formed for $v(t_0)/v_0 < 0$ and spikes formed for $v(t_0)/v_0 > 0$. The instability growth-rate is independent of the acceleration parameters, since the contributions of acceleration-induced terms to early-time dynamics are negligible⁴¹.

B. The late-time regime, $t - t_0 \gg \tau$

In the later-time regime, spikes are singular (the singularity is finite-time), whereas bubbles are regular^{5,15,25}. For $t \gg \tau$,

higher order harmonics are retained in the expressions for the moments, and regular asymptotic solutions are derived. We find asymptotic solutions for the relevant equations and determine their stability. We assume asymptotic solutions of the form

$$\frac{\zeta_1}{k} \sim \left(\frac{t}{\tau}\right)^\alpha, \quad \frac{M_n}{k^n}, \frac{\tilde{M}_n}{k^n} \sim \frac{1}{k\tau} \left(\frac{t}{\tau}\right)^\gamma, \quad (15)$$

where α and γ are constants to be determined. Substitution into Eqs. (8) and (9) lead, respectively, to the requirements that

$$\alpha - 1 = \alpha + \gamma = \gamma, \quad \gamma - 1 = 2\gamma.$$

That is,

$$\alpha = 0, \quad \gamma = -1.$$

We investigate the stability of these nonlinear asymptotic solutions by considering perturbations

$$\zeta_1(t) \rightarrow \zeta_1 + \delta\zeta_1(t)$$

$$M_j(t) \rightarrow M_j(t) + \delta M_j(t), \quad \tilde{M}_j(t) \rightarrow \tilde{M}_j(t) + \delta \tilde{M}_j(t)$$

with

$$\frac{\delta M_n}{M_n} \sim \frac{\delta \tilde{M}_n}{\tilde{M}_n} \sim \frac{\delta \zeta_1}{\zeta_1} \sim \left(\frac{t}{\tau}\right)^\beta. \quad (16)$$

Nonlinear asymptotic solutions are stable for $\text{Re}[\beta] < 0$ and are unstable otherwise.

Substituting the asymptotic forms Eq. (16) into Eqs. (8) and (9), employing a dominant balance argument and solving the resulting set of equations, at $N = 1$, we find a one-parameter family of solutions. We choose the bubble curvature ζ_1 to parameterise the family. The Fourier amplitudes are

$$\Phi_{10} = -\frac{2k + 8\zeta_1}{3k + 8\zeta_1} v, \quad \Phi_{20} = \frac{k + 8\zeta_1}{6k + 16\zeta_1} v,$$

$$\tilde{\Phi}_{10} = \frac{2k - 8\zeta_1}{3k - 8\zeta_1} v, \quad \tilde{\Phi}_{20} = \frac{-k + 8\zeta_1}{6k - 16\zeta_1} v,$$

$$-v = 2\Phi_{10} + 2\Phi_{20}, \quad v = 2\tilde{\Phi}_{10} + 2\tilde{\Phi}_{20}. \quad (17)$$

While these expressions are identical to those for the $a > -2$ case, and are repeated here for the convenience of the reader, the velocity and shear solutions are very different from those obtained in the $a > -2$ case⁴¹. Specifically, the velocity is

$$\hat{v} = \frac{A(9 - 64\hat{\zeta}^2)(128A\hat{\zeta}^3 - 10A\hat{\zeta} + 3)}{3(64A\hat{\zeta}^2 + 9A + 48\hat{\zeta})},$$

where

$$\hat{v} = \frac{Aktv(t)}{3}, \quad \hat{\zeta} = -\frac{\zeta_1}{k} > 0, \quad (18)$$

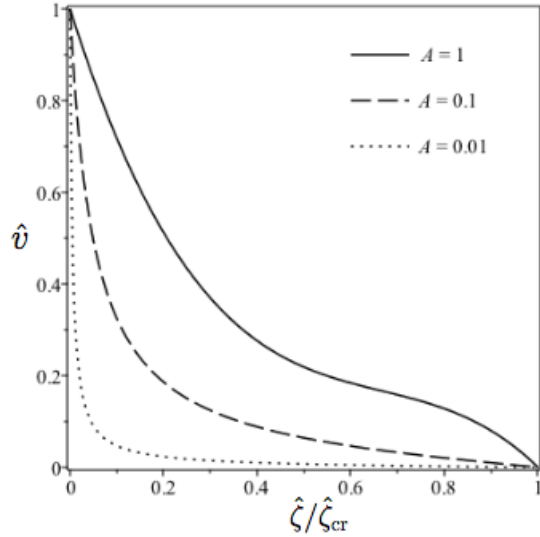


FIG. 1. Bubble tip velocity as a function of curvature for various Atwood numbers

We may likewise scale the harmonics:

$$\hat{\Phi}_{mn} = \frac{Akt\Phi_{mn}(t)}{3}, \quad \hat{\tilde{\Phi}}_{mn} = \frac{Akt\tilde{\Phi}_{mn}(t)}{3}.$$

For $\hat{\zeta}$ small, specifically $\hat{\zeta} \ll \frac{\sqrt{5}}{8}$,

$$\hat{v} \approx 1 - \frac{10A^2 + 16}{3A} \hat{\zeta}.$$

For bubbles, $\zeta < 0$ and $\nu > 0$ in which case solutions will exist for $\hat{\zeta} \in (0, \hat{\zeta}_{cr})$ where $\hat{\zeta}_{cr} = \frac{3}{8}$ with corresponding $\zeta_{cr} = -\frac{3}{8}k$. Fig. 1 shows the bubble tip velocity as a function of the bubble curvature. In the limits $A \rightarrow 0^+$ and $A \rightarrow 1^-$, the velocities become, respectively,

$$\hat{v}_{A=0}(t) = \frac{9 - 64\hat{\zeta}^2}{16kt\hat{\zeta}}, \quad \hat{v}_{A=1}(t) = \frac{(3 - 8\hat{\zeta})(16\hat{\zeta}^2 - 6\hat{\zeta} + 1)}{kt}.$$

Figs. 2 and 3 are plots of $\psi_{m0} = \ln \left| \frac{\Phi_{m0}}{\Phi_{10\max}} \right|$ and $\tilde{\psi}_{m0} = \ln \left| \frac{\tilde{\Phi}_{m0}}{\tilde{\Phi}_{10\max}} \right|$ as functions of ζ/ζ_{cr} for Atwood number $A = \frac{2}{3}$, and demonstrate that the second Fourier amplitude is much smaller than the first for $\hat{\zeta} < \hat{\zeta}_{cr}$. We note that $\Phi_{10} = \Phi_{20}$ when $\hat{\zeta} = \frac{5}{24}$. This defines the convergence limit and we refer to the bubble with this curvature as the ‘convergence bubble’.

Solutions for $N > 1$ can likewise be calculated. The resultant expressions are cumbersome^{5,14,15,25,27,38,39} and not given here. Similarly to these cited works, the solutions converge for increasing N and in each case the lowest order harmonics are dominant

C. The effect of shear

The multiplicity of these nonlinear asymptotic solutions is also due to the presence of shear at the interface, as suggested

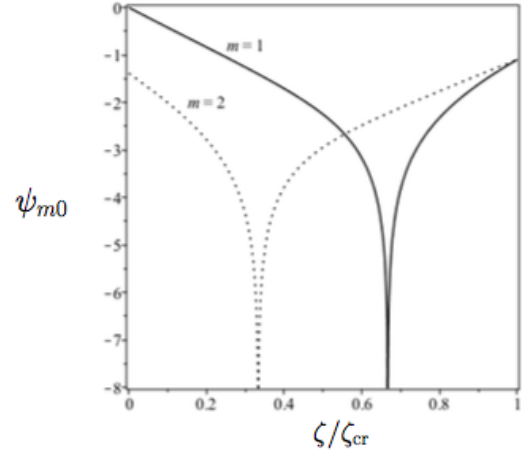


FIG. 2. ψ_{m0} for the heavy fluid

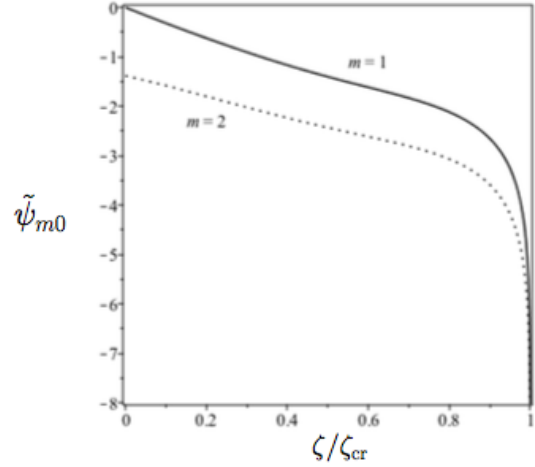


FIG. 3. ψ_{m0} for the light fluid

by the boundary conditions Eq. (10). We define shear function Γ to be the spatial derivative of the jump in the tangential velocity across the interface. We find that in the vicinity of the bubble tip it is $\Gamma = \tilde{M}_1 - M_1$. Specifically,

$$\hat{\Gamma} = \frac{9\hat{v}}{9 - 64\hat{\zeta}^2} = \frac{3A(128A\hat{\zeta}^3 - 10A\hat{\zeta} + 3)}{64A\hat{\zeta}^2 + 9A + 48\hat{\zeta}}, \quad (19)$$

where

$$\hat{\Gamma}(t) = \frac{At}{2}\Gamma.$$

For $\hat{\zeta}$ small, specifically $\hat{\zeta} \ll \frac{\sqrt{5}}{8}$,

$$\hat{\Gamma} \approx 1 - \frac{10A^2 + 16}{3A} \hat{\zeta}$$

Fig. 4 shows the interface shear function versus the bubble curvature. For Atwood numbers exceeding $A^* = \frac{2}{9}$ the shear

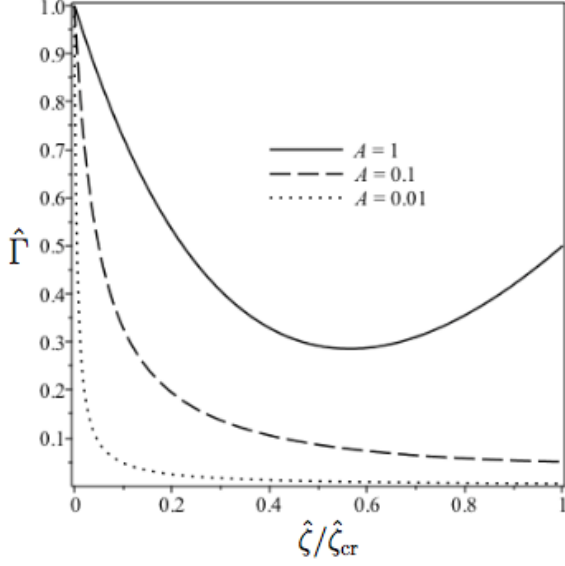


FIG. 4. Shear as a function of curvature for various Atwood numbers

function is concave upwards, and for values $A < A^*$ it is monotone decreasing. When $A = 1$, the shear function achieves its minimum value of $\hat{\Gamma} = \frac{6\sqrt{22}-27}{4}$ at $\frac{\hat{\zeta}}{\hat{\zeta}_{cr}} = \frac{\sqrt{22}-3}{3}$ and the corresponding velocity is $\hat{v} = \frac{231-49\sqrt{22}}{18}$.

For Atwood numbers $A > A^*$, the shear function attains a minimum value $\hat{\Gamma}_{min}$ at some curvature value $\hat{\zeta}_{min}$ and consequently, there are two branches of solutions. For small curvatures $\hat{\zeta} < \hat{\zeta}_{min}$, less curved bubbles experience greater shear whereas for large curvatures $\hat{\zeta} > \hat{\zeta}_{min}$, less curved bubbles experience less shear.

Fig. 5 shows the interface shear function versus the bubble tip velocity. For Atwood numbers $A > A^*$, the situation is as follows: For small curvatures $\hat{\zeta} < \hat{\zeta}_{min}$, faster bubbles experience less shear whereas for large curvatures, $\hat{\zeta} > \hat{\zeta}_{min}$, faster bubbles experience more shear.

D. Special solutions

There are a number of solutions in the family that deserve special attention. These are the fastest bubble, the Taylor bubble, the convergence bubble, the minimum-shear bubble, and the critical bubble.

1. The Atwood bubble

The fastest member of the family we refer to as the ‘Atwood bubble’ to emphasise its dependence on the Atwood number. The velocity is $\hat{v}_A = 1$, the shear function is $\hat{\Gamma}_A = 1$, and the harmonics are $\hat{\Phi}_{10A} = -\frac{2}{3}\hat{v}_A$, $\hat{\Phi}_{20A} = \frac{1}{6}\hat{v}_A$, $\hat{\Phi}_{10A} = \frac{2}{3}\hat{v}_A$, $\hat{\Phi}_{20A} = -\frac{1}{6}\hat{v}_A$. We note that this is in fact the flat bubble.

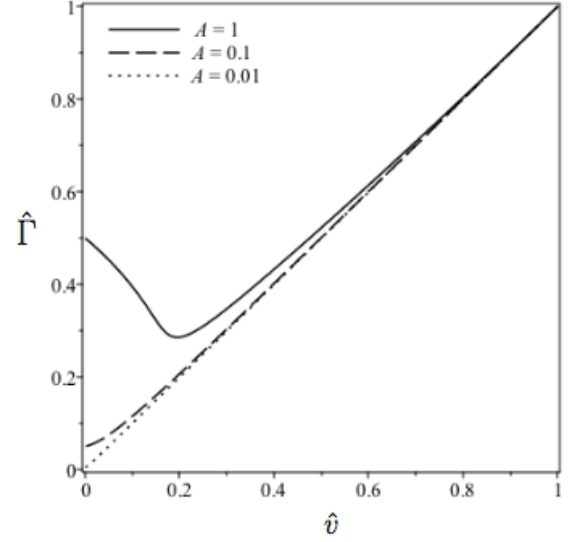


FIG. 5. Bubble tip velocity as a function of shear for various Atwood numbers

2. The Taylor bubble

We refer to this bubble as a ‘Taylor bubble’ since its curvature is the same as in the work⁴ except for a difference in the wavevector value. For the Taylor bubble the curvature, velocity and shear function are

$$\hat{\zeta}_T = \frac{1}{8}, \quad \hat{v}_T = \frac{4A(3-A)}{3(3+5A)}, \quad \hat{\Gamma}_T = \frac{9}{8}\hat{v}_T. \quad (20)$$

The corresponding Fourier amplitudes are $\hat{\Phi}_{10T} = -\frac{1}{2}\hat{v}_T$, $\hat{\Phi}_{20T} = 0$, $\hat{\Phi}_{10T} = \frac{3}{4}\hat{v}_T$ and $\hat{\Phi}_{20T} = -\frac{1}{4}\hat{v}_T$. Note that $\hat{\Phi}_{20T} \neq 0$ for $N > 1^{5,14,15,25,27,38,39}$.

3. The convergence bubble

The magnitudes of the Fourier harmonics $|\Phi_{10}(t)|$ and $|\Phi_{20}(t)|$ coincide when $\hat{\zeta} = \frac{5}{24}$. This defines the convergence limit. For the convergence bubble the curvature, velocity and shear function are

$$\hat{\zeta}_{CL} = \frac{5}{24}, \quad \hat{v}_{CL} = \frac{28A(81-25A)}{81(45+53A)}, \quad \hat{\Gamma}_{CL} = \frac{81}{56}\hat{v}_{CL}. \quad (21)$$

The corresponding Fourier amplitudes are $\hat{\Phi}_{10CL} = -\frac{1}{4}\hat{v}_{CL}$, $\hat{\Phi}_{20CL} = -\frac{1}{4}\hat{v}_{CL}$, $\hat{\Phi}_{10CL} = \frac{11}{14}\hat{v}_{CL}$ and $\hat{\Phi}_{20CL} = -\frac{2}{7}\hat{v}_{CL}$.

4. The minimum-shear bubble

When $A = 1$ the shear function achieves its minimum value $\hat{\Gamma} = \frac{6\sqrt{22}-27}{4}$ at $\frac{\hat{\zeta}}{\hat{\zeta}_{cr}} = \frac{\sqrt{22}-3}{3}$, and the corresponding velocity

is $\hat{v} = \frac{231-49\sqrt{22}}{18}$. For A values slightly below $A = 1$, the shear function achieves its minimum value at

$$\frac{\hat{\zeta}}{\hat{\zeta}_{\text{cr}}} = \frac{\sqrt{22}-3}{3} + \frac{1}{5}(1-A).$$

When $A = \frac{2}{9}$, the minimum value for which the shear achieves a minimum in $(0, \hat{\zeta}_{\text{cr}})$, the shear function achieves its minimum value of $\hat{\Gamma} = \frac{1}{9}$ at $\frac{\hat{\zeta}}{\hat{\zeta}_{\text{cr}}} = 1$, and the corresponding velocity is $\hat{v} = 0$. For A values slightly above $A = \frac{2}{9}$, the shear function achieves its minimum value at

$$\frac{\hat{\zeta}}{\hat{\zeta}_{\text{cr}}} = 1 - \frac{81}{50} \left(A - \frac{2}{9} \right).$$

5. The critical bubble

For the critical bubble the curvature, velocity and shear function are

$$\hat{\zeta}_{\text{Cr}} = \frac{3}{8}, \quad \hat{v}_{\text{Cr}} = 0, \quad \hat{\Gamma}_{\text{Cr}} = \frac{A}{2}. \quad (22)$$

The corresponding Fourier amplitudes are $\hat{\Phi}_{10\text{Cr}} = \frac{A}{3}$, $\hat{\Phi}_{20\text{Cr}} = -\frac{A}{3}$, $\hat{\Phi}_{10\text{Cr}} = 0$, $\hat{\Phi}_{20\text{Cr}} = 0$. Note that $\hat{\Phi}_{10\text{Cr}} \neq 0$ and $\hat{\Phi}_{20\text{Cr}} \neq 0$ for $N > 1$.

E. Stability

The stability variable β satisfies a quadratic equation which does not depend on the value of the acceleration exponent a . The analytical result is too cumbersome to be presented here. Fig 6 shows the stability function for various Atwood numbers. We observe that all bubbles up to the convergence limit $\hat{\zeta}_{\text{CL}}/\hat{\zeta}_{\text{cr}} = \frac{5}{9}$ are stable at $N = 1$. The $N > 1$ analysis is to be presented elsewhere.

F. Properties of nonlinear RM dynamics

1. Multiscale character of RM dynamics

The multi-scale character of the dynamics can be understood by viewing the RM coherent structure as a standing wave with growing amplitude³⁵. The multi-scale character of nonlinear RMI is consistent with the existence of an amplitude scale in early-time shock-driven RMI, at which the maximum initial growth-rate of RMI is achieved¹⁸.

The Atwood (flat) bubble is the fastest stable solution and is hence the physically significant solution. This solution has the (quasi) invariant value

$$\frac{tv_{\text{F}}^2}{\left(\frac{dv_{\text{F}}}{d\zeta}\right)_{\zeta=0}} = \frac{9}{16 + 10A^2}.$$

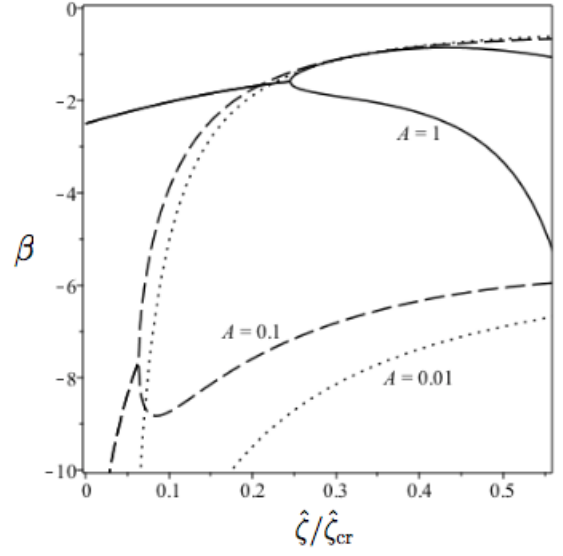


FIG. 6. Stability profiles for various Atwood numbers

This (quasi) invariance implies that nonlinear RM dynamics is multi-scale, with two macroscopic length scales contributing. These being the wavelength and the amplitude^{5,15,25}.

2. Interfacial character of RM dynamics

By accurately accounting for the interplay of harmonics and by systematically connecting the interfacial velocity and shear for a broad range of acceleration parameters, we have found that RM dynamics is essentially interfacial: It has intense fluid motion in the vicinity of the interface and effectively no motion away from the interface. The velocity is potential in the bulk of each fluid. Shear-driven vortical structures may appear at the interface. Fig. 7 shows the qualitative velocity field in the laboratory reference frame in the (x, z) -plane of the $\hat{\zeta} = 1/10$ bubble for Atwood number $A = 2/3$ at time $t = 1$, for any $a < -2$. Shear-driven vortical structures may appear at the interface due to discontinuity of the tangential component of velocity. Near the tip of the bubble the vortical structures ‘rotate’ from the heavy to the light fluid. This velocity pattern is observed in experiments and simulations, demonstrating qualitative agreement with our results^{2,14,20,21,31–33}.

IV. DISCUSSION

Our theory finds that in RMI with variable acceleration, nonlinear bubbles decelerate and flatten. This behaviour is observed in experiments and simulations, in agreement with our results^{5,6,14–20}. According to our theory, in nonlinear RMI with variable acceleration, flattened bubbles move more quickly and decelerate more rapidly when compared to curved bubbles because since the bubble velocity decays with time as

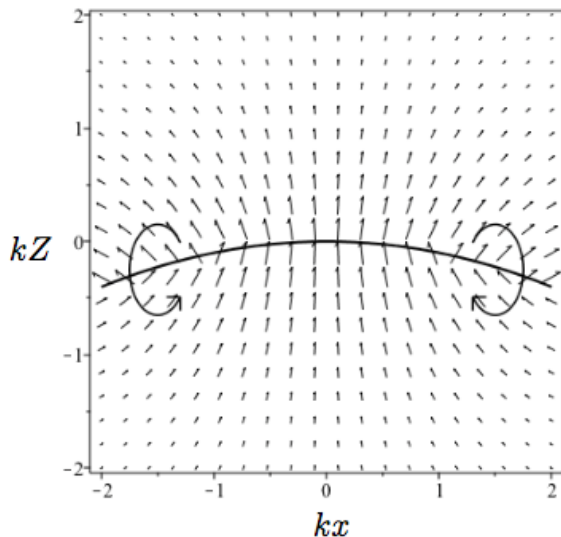


FIG. 7. Qualitative velocity field of the Atwood bubble in the plane $y = 0$ in the laboratory reference frame, $Z = z - z_0(t)$. The curved arrows indicate that near the tip of the bubble the vortical structures ‘rotate’ from the heavy to the light fluid.

C/kt , the deceleration is $-C/kt^2$. Moreover, according to our results, RM bubbles move more quickly and have larger interfacial shear for fluids with similar densities than for fluids with very different densities^{6,15,20,29,34,37}. This result has a clear interpretation: for fluids with similar densities, shear-driven interfacial vortical structures are more intense, leading to stronger energy dissipation, stronger deceleration and thus, to larger bubble velocity when compared to fluids with very different densities.

Our analysis is focused on large-scale dynamics, presuming that interfacial vortical structures are small. This assumption is applicable for fluids of very different densities and with a finite density ratio. For fluids with very similar densities $A \rightarrow 0^+$ other approaches should be employed^{5,14,15,25,27}. While for fluids with very similar densities our theory is no longer applicable, the singular nature of the velocity of the fastest stable bubble for $A \rightarrow 0^+$ indicates that for $A \rightarrow 0^+$ and $t/\tau \rightarrow \infty$ the bubble velocity may decay more quickly than inverse time^{5,6,15,20,25,40}.

According to our results, for variable acceleration with $a < -2$, RM dynamics depends on the initial conditions and is independent of the acceleration. Hence, one can scrupulously study the effect of initial conditions on RM dynamics by analyzing properties of the unstable interface for various accelerations^{8–14}. Note that accurate quantification of nonlinear RMI in observations may be a challenge because the interface velocity is usually of the order of 0.1% of the largest velocity scale in the post-shock fluid system, and because the interface velocity is a power-law function of time, which requires a substantial span of temporal and spatial scales for accurate diagnostics^{15–20}.

In addition to determining the interface velocity, we have elaborated theory benchmarks which have not been discussed

before. These are the fields of velocity and pressure, interface morphology and bubble curvature, interfacial shear and its link to the bubble velocity and curvature, and spectral properties of the velocity and pressure. By diagnosing the dependence of these quantities on the density ratios, flow symmetries, initial conditions, and accelerations, by identifying their universal properties, and by accurately measuring departures of data in real fluids from theoretical solutions in ideal fluids, one can further advance knowledge of RM dynamics in realistic environments, better understand RM relevant processes in nature and technology, and improve methods of numerical modeling and experimental diagnostics of RM dynamics in fluids, plasmas, and materials.

To conclude, we have considered the long-standing problem of RMI with variable acceleration by applying group theory. We have directly linked the interface velocity, morphology and shear, revealed the interfacial and multi-scale character of RM dynamics, achieved good agreement with available observations, and elaborated new theory benchmarks for future experiments and simulations.

V. ACKNOWLEDGEMENTS

The authors thank the University of Western Australia (AUS) and the National Science Foundation (USA).

VI. REFERENCES

- ¹R. D. Richtmyer, *Commun Pure Appl Math* **13**, 297 (1960).
- ²E. E. Meshkov, *Sov Fluid Dyn* **4**, 101 (1969).
- ³L. Rayleigh, *Proc London Math Soc* **14**, 170 (1883).
- ⁴R. M. Davies and G. I. Taylor, *Proc R Soc A* **200**, 375 (1950).
- ⁵S. I. Abarzhi, *Phil Trans R Soc A* **368**, 1809 (2010).
- ⁶E. E. Meshkov, *Studies of hydrodynamic instabilities in laboratory experiments* (Sarov, 2006).
- ⁷S. I. Abarzhi, S. Gauthier, and K. R. Sreenivasan, *Turbulent mixing and beyond: non-equilibrium processes from atomistic to astrophysical scales. I & II* (Royal Society Publishing, 2013).
- ⁸D. Arnett, *Supernovae and Nucleosynthesis: An Investigation of the History of Matter, from the Big Bang to the Present* (Princeton University Press, 1996).
- ⁹Y. B. Zeldovich and Y. P. Raizer, *Physics of shock waves and high-temperature hydrodynamic phenomena* (Dover New York, 2002).
- ¹⁰S. W. Haan, *Phys. Plasmas* **18**, 051001 (2011).
- ¹¹N. Peters, *Turbulent Combustion* (Cambridge University Press, 2000).
- ¹²S. Rana and M. Herrmann, *Phys Fluids* **23**, 091109 (2011).
- ¹³M. J. Buehler, H. Tang, A. C. T. van Duin, and W. A. Goddard, *Phys Rev Lett* **99**, 165502 (2007).
- ¹⁴S. I. Abarzhi, A. Bhowmick, A. Naveh, A. Pandian, N. Swisher, R. Stellingwerf, and W. Arnett, *Proc Natl Acad Sci USA*, 201714502 (2018).
- ¹⁵S. I. Abarzhi, *Physica Scripta* **2008** (T132), 014012 (2008).
- ¹⁶M. Stanic, R. F. Stellingwerf, J. T. Cassibry, and S. I. Abarzhi, *Phys Plasmas* **19**, 082706 (2012).
- ¹⁷Z. Dell, R. F. Stellingwerf, and S. I. Abarzhi, *Phys Plasmas* **22**, 092711 (2015).
- ¹⁸Z. Dell *et al.*, *Phys Plasmas* **24**, 090702 (2017).
- ¹⁹A. Pandian, R. F. Stellingwerf, and S. I. Abarzhi, .
- ²⁰E. E. Meshkov, *Phil Trans R Soc A* **371**, 20120288 (2013).
- ²¹H. F. Robey, Y. Zhou, A. C. Buckingham, P. Keiter, B. A. Remington, and R. P. Drake, *Phys. Plasmas* **10**, 614 (2003).
- ²²S. Lugomer, *Laser Part. Beams* **34**, 123 (2016).

- ²³N. Swisher *et al.*, *Phys. Plasmas* **22**, 102707 (2015).
- ²⁴S. S. Orlov, S. I. Abarzhi, S.-B. Oh, G. Barbastathis, and K. R. Sreenivasan, *Phil Trans R Soc A* **368**, 1705 (2010).
- ²⁵S. I. Anisimov, R. P. Drake, S. Gauthier, E. E. Meshkov, and S. I. Abarzhi, *Phil Trans R Soc A* **371**, 20130266 (2013).
- ²⁶H. J. Kull, *Phys Rep* **206**, 197 (1991).
- ²⁷S. I. Abarzhi, *Phys Rev Lett* **81**, 337 (1998).
- ²⁸K. Nishihara, J. G. Wouchuk, C. Matsuoka, R. Ishizaki, and V. V. Zakhovskiy, *Phil Trans R Soc A* **368**, 1769 (2010).
- ²⁹A. K. Bhowmick and S. I. Abarzhi, *Phys Plasmas* **23**, 112702 (2016).
- ³⁰S. Gauthier and B. L. Creurer, *Phil Trans R Soc A* **368**, 368:1681 (2010).
- ³¹K. Kadau, J. L. Barber, T. C. Germann, B. L. Holian, and B. J. Alder, *Phil Trans R Soc A* **368**, 1547 (2010).
- ³²J. Glimm, D. H. Sharp, T. Kaman, and H. Lim, *Phil Trans R Soc A* **371**, 20120183 (2013).
- ³³D. L. Youngs, *Phil Trans R Soc A* **371**, 20120173 (2013).
- ³⁴B. Thornber *et al.*, *Phys Fluids* **29**, 105107 (2017).
- ³⁵L. D. Landau and E. M. Lifshitz, *Course of Theoretical Physics* (Pergamon Press, New York, 1987).
- ³⁶L. I. Sedov, *Similarity and dimensional methods in mechanics* (CRC Press, 1993).
- ³⁷D. L. Hill, A. K. Bhowmick, D. V. Ilyin, and S. I. Abarzhi, *Phys Rev Fluids* **4**, 063905 (2019).
- ³⁸P. R. Garabedian, *Proc R Soc A* **241**, 423 (1957).
- ³⁹N. A. Inogamov, *JETP Lett* **55**, 521 (1992).
- ⁴⁰S. I. Abarzhi, K. Nishihara, and J. Glimm, *Phys Lett A* **317**, 470 (2003).
- ⁴¹D. L. Hill, A. K. Bhowmick, and S. I. Abarzhi, *arXiv*, 1903.08151 (2019).